Lamellar biogels comprising fluid membranes with a newly synthesized class of polyethylene glycol-surfactants

Heidi E. Warriner, Patrick Davidson,[a] and Nelle L. Slack
Materials Research Laboratory, Materials Department and Physics Department, Biochemistry and Molecular Biology Program, University of California, Santa Barbara, California 93106

Matthias Schellhorn[b]
Makromolekulare Chemie I and Bayreuther Institut für Makromolekülforschung (BIMF), Universität Bayreuth, 95440 Bayreuth, Germany

Petra Eiselt and Stefan H. J. Idziak[c]
Materials Research Laboratory, Materials Department and Physics Department, Biochemistry and Molecular Biology Program, University of California, Santa Barbara, California 93106

Hans-Werner Schmidt
Makromolekulare Chemie I and Bayreuther Institut für Makromolekülforschung (BIMF), Universität Bayreuth, 95440 Bayreuth, Germany

Cyrus R. Safinya[d]
Materials Research Laboratory, Materials Department and Physics Department, Biochemistry and Molecular Biology Program, University of California, Santa Barbara, California 93106

(Received 29 January 1997; accepted 9 May 1997)

A series of four polymer–surfactant macromolecules, each consisting of a double-chain hydrophobic moiety attached onto a monofunctional polyethylene glycol (PEG) polymer chain, were synthesized in order to study their effect upon the fluid lamellar liquid crystalline (L_α) phase of the dimyristoylphosphatidylcholine/pentanol/water system. The main finding of this study is that the addition of these compounds induces a new lamellar gel, called $L_{\alpha,g}$. We have determined the phase diagrams as a function of PEG–surfactant concentration, c_{PEG}, and weight fraction water, Φ_W. All phase diagrams are qualitatively similar and show the existence of the gel. Unlike more common polymer physical gels, this gel can be induced either by increasing c_{PEG} or by adding water at constant c_{PEG}. In particular, less polymer is required for gelation as water concentration increases. Moreover, the gel phase is attained at concentrations of PEG–surfactant far below that required for classical polymer gels and is stable at temperatures comparable to the lower critical solution temperature of free PEG–water mixtures. Small angle x-ray experiments demonstrate the lamellar structure of the gel phase, while wide angle x-ray scattering experiments prove that the structure is L_α, not $L_{\beta'}$ (a common chain-ordered phase which is also a gel). The rheological behavior of the $L_{\alpha,g}$ phase demonstrates the existence of three dimensional elastic properties. Polarized light microscopy of $L_{\alpha,g}$ samples reveals that the $L_{\alpha,g}$ is induced by a proliferation of defect structures, including whispy lines, spherulitic defects, and a nematiclike Schlieren texture. We propose a model of topological defects created by the aggregation of PEG–surfactant into highly curved regions within the membranes. This model accounts for both the inverse relationship between Φ_W and c_{PEG} observed along the gel transition line and the scaling dependence of the interlayer spacing at the gel transition with the PEG molecular weight. These L_α hydrogels could serve as the matrix for membrane-anchored peptides, proteins or other drug molecules, creating a ''bioactive gel'' with mechanical stability deriving from the polymer–lipid minority component.
 [S0021-9606(97)50431-4]

I. INTRODUCTION

A new kind of physical gel has recently been discovered[1,2] by adding a polyethylene glycol (PEG) containing polymer–surfactant to the classical liquid crystalline L_α phase of the biological surfactant dimyristoylphosphatidylcholine (DMPC) and the cosurfactant pentanol dissolved in water. This polymer–surfactant, PEG-DMPE, was obtained by attaching the lipid dimyristoylphosphatidylethanolamine (DMPE) at one end of a water soluble polyethylene glycol polymer chain. Figure 1 schematically illustrates undulating fluid membranes composed of the lipid DMPC, a cosurfactant pentanol and a PEG–surfactant. The hydrophobic moiety inserts inside the fluid lipid bilayers while the polyethylene glycol chain remains in the intermembrane aqueous region. Fluid membranes comprise the L_α phase,

[a]Permanent address: Laboratoire de Physique des Solides (CNRS), Bat. 510, Universite Paris Sud, 91405 Orsay, Cedex, France.
[b]Permanent address: Boehringer Ingelheim KG, 55216 Ingelheim, Germany.
[c]Permanent address: Department of Physics, University of Waterloo, Waterloo, Ontario N2L 3G1, Canada.
[d]Author to whom correspondence should be addressed.

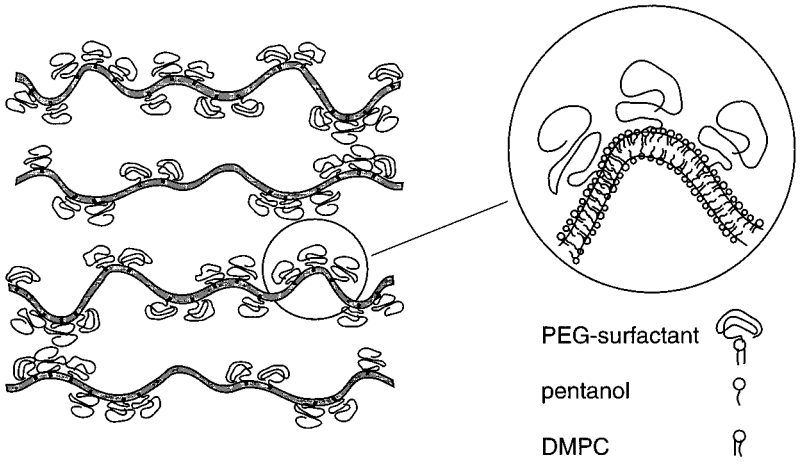

FIG. 1. Schematic representation of undulating fluid membranes composed of a lipid (DMPC), a cosurfactant (pentanol), and a PEG–surfactant.

allowing the PEG–surfactant molecules to diffuse freely across the plane of the membrane.

The new phase, hereafter called $L_{\alpha,g}$, has the same liquid crystalline lamellar symmetry as that of more common fluid L_α phases but displays the rheological properties of a gel. However, the $L_{\alpha,g}$ phase comprises lipid chains in the melted state and thus should not be confused with $L_{\beta'}$ phases[3] in which gel properties derive from in-plane ordering. In sharp contrast to the behavior of gels composed of free polymer plus a solvent, this lamellar biogel requires less polymer–surfactant to achieve gelation as water content increases. The $L_{\alpha,g}$ phase is even stable at elevated temperatures (90–120 °C), comparable to the lower critical solution temperature of low molecular weight free PEG–water mixtures.[4] A significant finding is the formation of lamellar gels containing just 0.5 wt. % PEG-lipid, much less than a monolayer coverage of the bilayers. A free-polymer hydrogel at this concentration would require a PEG molecular weight of order a million. Another unusual feature of the $L_{\alpha,g}$ is that it forms from a liquidlike L_α phase through the addition of water, but dissolves back into a flowing two-phase liquid through the further addition of water. In short, the $L_{\alpha,g}$ does not arise from the direct entanglement of polymer chains because it obtains only at very low PEG–surfactant concentrations and at lamellar spacings much larger than the PEG radius of gyration R_g.

The occurrence of this gel was explained by the nucleation and proliferation of topological defects[1,2] whose free energy cost is reduced by the influence of the polymer–surfactant on the spontaneous curvature of the layers. Recent freeze-fracture and polarizing optical microscopy studies reveal that the microstructure of the $L_{\alpha,g}$ consists of a variety of liquid crystalline defects tethered together by shared membrane sheets: anisotropic and isotropic spherulites, crescents, and edge dislocation defects were clearly observed.[5]

Related studies[6] have dealt with the interactions of free water-soluble polymers with bilayers of L_α phases. One of the main observations from these investigations is the coexistence of two L_α phases differing by their polymer concentrations. The system described in Refs. 1 and 2 and the present study is distinct in that the PEG-containing polymer–surfactants are hydrophobically anchored to the lipid bilayers; at the concentrations studied, these polymer-surfactants do not engender phase separation. Furthermore, the molecular weight of the PEG chains used is kept relatively low (2000 and 5000 g/mol). The lipid system is uncharged so that the electrostatic interactions are not relevant; in addition, the cosurfactant pentanol is used to thin the membranes,[7] decreasing the value of the membrane bending rigidity κ to approximately k_BT. In large part these L_α phases are stabilized by long-range repulsive undulation forces.[2,7–9]

The low immunogenicity of polyethylene glycol makes it an attractive polymer for biomedical applications[10] and surfactants with covalently attached polyethylene glycol have been investigated in this light. In the field of drug delivery, PEG-coated liposomes, called ''Stealth'' liposomes, inhibit the body's immune system and have much longer circulation times in blood, conferring interesting drug carrier potentialities.[11–14] This increased lifetime is presently thought to result from a repulsive steric interaction due to the grafted polymer chains.[15] Interactions between PEG-coated membranes have actually been measured both for the L_α phase[16] and for chain frozen membranes deposited on a solid substrate.[17] These studies focussed on ''stiff'' ($\kappa \gg k_BT$) membranes, as opposed to the highly flexible system under consideration here; such systems do not appear to form the type of gel we report. However, PEG-based gels are generally interesting coatings for more immunogenic compounds[18] because PEG chains efficiently repel proteins and cells, shielding the substrate material. The PEG–surfactant-based gel described here could extend the utility of PEG by acting as the matrix for bioactive gels of enhanced mechanical stability. Unlike free-polymer gels or $L_{\beta'}$ gels which comprise solid membranes, this type of gel could be activated by the addition of membrane-embedded proteins.

In order to test the generality of the gelation phenomenon, we prepared a series of PEG–surfactant macromolecules, each consisting of a double chain hydrophobic moiety attached onto a monofunctional polyethylene glycol

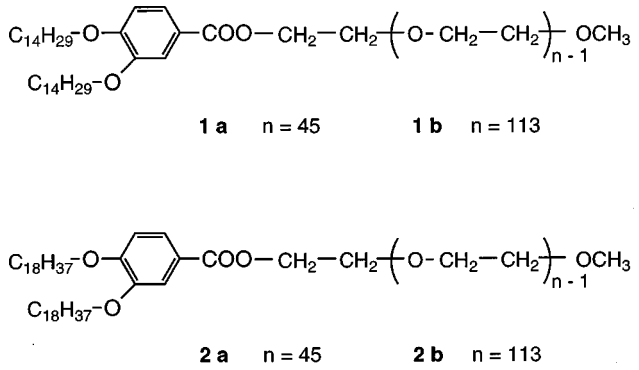

FIG. 2. Chemical structure of PEG–surfactants **1a**, **1b**, **2a**, and **2b** used in this study.

monomethyl ether. The chemical structures of PEG–surfactants are given in Fig. 2. The hydrophobic part is based on a 3,4-bis(alkoxy)benzoic acid moiety. Two different lengths of the *n*-alkyl chains (**1a,1b** $n=14$ and **2a,2b** $n=18$) were used in order to influence the hydrophobic interaction. The molecular weight of the attached poly(ethylene glycol) polymer chain was 2000 g/mol ($n=45$) for **1a,2a** and 5000 g/mol ($n=113$) for **1b,2b** respectively. In this paper, we show the effects of the addition of these new PEG–surfactants on the L_α phase of the dimyristoylphosphatidylcholine (DMPC)/pentanol/water system. Phase diagrams for all PEG–surfactants in terms of weight fraction water vs mol % PEG–surfactant (Φ_w vs c_{PEG}) were explored in order to characterize the L_α–$L_{\alpha,g}$ transition.

II. EXPERIMENT

Except where specified, measurements were carried out at ambient or ''room'' temperature (22–25 °C).

A. Materials

A series of four PEG–surfactants **1a**, **1b**, **2a**, and **2b** (Fig. 2) was synthesized by the coupling reaction of 3,4-bis(alkoxy)benzoic acid chloride with monofunctional poly(ethylene glycol) monomethylether of different molecular weights. For the synthesis poly(ethylene glycol) monomethylethers (Aldrich) with a number average molecular weight (M_n) of 2000 and 5000 g/mol were used. Gel permeation chromatography (GPC) in chloroform (standard: polystyrene) gave a polydispersity (M_w/M_n) of 1.13 and 1.11, respectively. The calculation of the molar weight of PEG–surfactants is based on the M_n values given by Aldrich and are **1a**: 2530 g/mol, **1b**: 5530 g/mol, **2a**: 2642 g/mol, and **2b**: 5642 g/mol. The detailed synthesis and characterization of these compounds and other PEG-containing surfactants will be published separately.[19]

DMPC of a purity >99% was purchased from Avanti Polar Lipids Inc., pentanol of 99%+purity was purchased from Sigma Chemical Co., both compounds were used as received. We also used the purified 18 MΩ water provided from a Millipore unit.

B. Sample preparations

All samples were prepared in 13 mm diam glass test tubes and carefully sealed. The tubes were first cleaned with a 2:1 vol/vol chloroform/methanol solution, rinsed once with spectroscopic grade ethanol, rinsed multiple times with Millipore water and left to dry in an oven.

A molar ratio of pentanol to surfactant molecules (DMPC+PEG–surfactant) of $4.0+/-0.5$ was maintained for all samples. This high ratio was used to ensure that the surfactant chains would always be in the melted state and that the bilayers formed would be sufficiently flexible to have a large undulation repulsion. We also fixed this ratio in order to isolate the effect of PEG–surfactant on membrane fluidity, bending rigidity, and shape. With this ratio fixed, the remaining compositional degrees of freedom are water content Φ_w (water weight fraction) and the molar ratio of PEG–surfactant to total surfactant molecules, c_{PEG} (expressed in %).

Samples were prepared by weighing in the appropriate amounts of lipid, pentanol, PEG–surfactant, and water. Pentanol was always added last. Samples were centrifuged to collect all compounds at the bottom of the tube and then subjected to approximately $\frac{1}{2}$ h of sonication to break up any clumping. After mixing with a Vortexer (Fisher Scientific, Tustin CA, USA) the samples were centrifuged again and left to stand for 1–4 weeks before phase determination. After the initial phase determination, samples were checked for any changes every few months. For a ''line'' of increasing water concentration, a homogeneous master batch was made and the appropriate amounts of water added. In certain cases we spot-checked our results with samples not prepared via the master-batch method along the same line.

C. Definitions and formulas

In order to visually distinguish between a fluid L_α phase and a $L_{\alpha,g}$ gel phase, we adopted the following ''operational'' definition of a gel: any sample which does not flow for at least 5 s after turning the test tube upside down. More quantitative rheometric tests were also performed and will be described in the next section.

Densities used in all calculations are water, $\rho_{\mathrm{H_2O}}=1.0$ g/cm^3; DMPC, $\rho_{\mathrm{DMPC}}=1.1$ g/cm^3 [Refs. 3(b) 20]; pentanol, $\rho_{\mathrm{pent}}=0.81$ g/cm^3; PEG in solution with water, $\rho_{\mathrm{H_2O+PEG}}=1.03$ g/cm^3 (Ref. 21); hydrophobic part of PEG–surfactant, $\rho_{\mathrm{phobic}}=\rho_{\mathrm{DMPC}}$. Molecular weights are denoted by the following symbols: DMPC: $\mathrm{MW_{DMPC}}$; pentanol: $\mathrm{MW_{pent}}$; PEG–surfactant: $\mathrm{MW_{PEG-surfactant}}$; PEG: $\mathrm{MW_{PEG}}$; hydrophobic part of PEG–surfactant: $\mathrm{MW_{phobic}}$. The headgroup areas for DMPC and pentanol are estimated as described in Ref. 2 to be $A_{\mathrm{head}}=72.8\pm.1$ Å^2 and A_{pentanol}, 12.7 ± 0.1 Å^2. The headgroup area of the surfactant part of the PEG–surfactants is assumed to be equal to that of DMPC.

For each of the phase diagrams, the relevant definitions given below are used. For all equations, g_x is the weight in grams of material x.

$$d=\frac{2\pi}{q_0}, \tag{1}$$

where q_0 = position of the first harmonic in the lamellar x-ray diffraction pattern. In this paper,

$$q\equiv\frac{4\pi}{\lambda}\sin\theta.$$

$$\Delta d=\frac{(\text{stepsize in x-ray scan})\times d^2}{\pi}, \tag{2}$$

where Δd is the uncertainty in the value of d.

$$\Phi_W=\frac{g_{\text{water}}}{g_{\text{total}}}. \tag{3}$$

$$c_{\text{PEG}}=\frac{\left(\frac{g_{\text{PEG-surfactant}}}{\text{MW}_{\text{PEG-surfactant}}}\right)}{\left(\frac{g_{\text{PEG-surfactant}}}{\text{MW}_{\text{PEG-surfactant}}}+\frac{g_{\text{DMPC}}}{\text{MW}_{\text{DMPC}}}\right)}. \tag{4}$$

$$\Phi_{\text{mem}_{\text{PEG}}}=\frac{\left(\frac{g_{\text{PEG-surfactant}}}{\text{MW}_{\text{PEG-surfactant}}}\right)\times\left[\left(\frac{\text{MW}_{\text{PEG}}}{\rho_{\text{H}_2\text{O+PEG}}}\right)+\left(\frac{\text{MW}_{\text{phobic}}}{\rho_{\text{phobic}}}\right)\right]}{\left\{\left(\frac{g_{\text{PEG-surfactant}}}{\text{MW}_{\text{PEG-surfactant}}}\right)\times\left[\left(\frac{\text{MW}_{\text{PEG}}}{\rho_{\text{H}_2\text{O+PEG}}}\right)+\left(\frac{\text{MW}_{\text{phobic}}}{\rho_{\text{phobic}}}\right)\right]+\frac{g_{\text{DMPC}}}{\rho_{\text{DMPC}}}+\left(\frac{g_{\text{pent}}}{\rho_{\text{pent}}}\right)\times\left[1-g_{\text{H}_2\text{O}}\left(\frac{0.026}{0.974}\right)\right]\right\}}. \tag{5}$$

Qualitatively, $\Phi_{\text{mem}_{\text{PEG}}}$ is the volume fraction of membrane occupied by the polymer–surfactant.

We also use the classical relationship between the intermembrane spacing d and the volume fraction of membrane Φ_{mem} to find δ, the bilayer thickness.

$$\delta=d\times\Phi_{\text{mem}}, \tag{6}$$

where

$$\Phi_{\text{mem}}=\frac{\left\{\frac{(g_{\text{PEG-surfactant}})\times\left(\frac{\text{MW}_{\text{phobic}}}{\text{MW}_{\text{PEG-surfactant}}}\right)}{\rho_{\text{phobic}}}+\left(\frac{g_{\text{DMPC}}}{\rho_{\text{DMPC}}}\right)+\left[1-g_{\text{H}_2\text{O}}\left(\frac{0.026}{0.974}\right)\right]\times\left(\frac{g_{\text{pent}}}{\rho_{\text{pent}}}\right)\right\}}{\left\{\frac{(g_{\text{PEG-surfactant}})\times\left(\frac{\text{MW}_{\text{phobic}}}{\text{MW}_{\text{PEG-surfactant}}}\right)}{\rho_{\text{phobic}}}+\left(\frac{g_{\text{DMPC}}}{\rho_{\text{DMPC}}}\right)+\left(\frac{g_{\text{pent}}}{\rho_{\text{pent}}}\right)+\frac{\left[(g_{\text{PEG-surfactant}})\times\left(\frac{\text{MW}_{\text{PEG}}}{\text{MW}_{\text{PEG-surfactant}}}\right)+g_{\text{H}_2\text{O}}\right]}{\rho_{\text{H}_2\text{O+PEG}}}\right\}}. \tag{7}$$

In Eqs. (5) and (7), the factor of $[1-g_{\text{H}_2\text{O}}(0.026/0.974)]$ multiplying the pentanol volume takes into account the 2.6 w/w % solubility of pentanol in water.[22] In Eq. (5), the volume fraction of PEG–surfactant in the bilayer includes the polyethylene glycol moiety of the polymer–surfactant as part of the bilayer while in Eq. (7), the polymer part of the PEG–surfactant is excluded from the calculation of the volume fraction of the membrane. This paradox results from the dual nature of the PEG–surfactant; (1) it acts to swell the intermembrane distance like an equivalent volume of solvent, hence in the theoretical relationship between δ and d, it should be counted as part of the solvent but (2) the PEG–surfactant has a much larger headgroup to chain area ratio (Fig. 1) than either DMPC or pentanol, and hence can be expected to prefer a higher spontaneous curvature. We use Eq. (7) to express the first idea and Eq. (5) to express the second.

D. X-ray diffraction

X-ray scattering studies were performed on a Huber four-circle diffractometer using an 18 kW Rigaku rotating anode generator (Rigaku, Danvers, MA) (Cu K_α, $\lambda=1.54$ Å), a cylindrically bent focusing pyrolitic graphite (002) monochromator and a Bicron point detector (Bicron, Newbury, OH, USA). The in-plane resolution, defined using slits, was $\delta q=0.01-0.015$ Å^{-1}, and the out-of-plane resolution was $\delta q=0.14-0.3$ Å^{-1}; scan stepsize was generally 0.001 Å^{-1}. Additional experiments were carried out at the Stanford Synchrotron Radiation Laboratory on beamline 10-2 using either a Bicron point detector or a 180 mm MAR image-plate 2D x-ray detector (Mar Industries, San Diego, CA, USA). A Si (111) double bounce monochromator was used at 8 keV with focus at the sample position. In the Bicron experiments, in-plane resolution, again defined by slits, was $\delta q=0.0014-0.0028$ Å^{-1}, and the out-of-plane resolution was $\delta q=0.01-0.02$ Å^{-1}; scan stepsize was usually

$0.0005\,\text{Å}^{-1}$. For the 2D detector experiments, resolution was defined by the detector pixel size and the distance from sample to detector. Images were radially averaged to produce powder scans with a stepsize of $0.0007\,\text{Å}^{-1}$ and a radially averaged resolution of $0.0027\,\text{Å}^{-1}$. Exposure times were typically 1–2 h.

For all experiments, samples were sealed in either quartz or glass 1.5 mm x-ray capillary tubes (Charles Supper Co., Natick MA, USA). These capillary tubes were then set on a translation stage for automatic data acquisition. We found it necessary to heat and quench some fluid samples to obtain the proper isotropic distribution of lamellar domains.

E. Rheology

Constant-stress oscillatory shear-strain experiments were carried out with a Rheometrics dynamic stress rheometer, model 1710C (Rheometrics, Piscataway, NJ, USA), in the cone and plate geometry with a 40 mm diam plate, a cone angle of 0.04 rad, and a gap size of 0.05 mm. For this geometry, a volume of $0.7\,\text{cm}^3$ is recommended. In our experiments, a volume of $1-1.5\,\text{cm}^3$ was used. In order to minimize evaporation during testing, a small housing was placed around the set up which enclosed pentanol and water-soaked cotton balls. All experiments were performed at room temperature.

Samples were subjected to three different tests. In order to establish the regime of linear viscoelasticity, we performed a dynamic stress sweep test in which the stress is increased from about 0.6 to 100 dyn/cm^2 at a frequency of 1 Hz. Within this regime, each sample was tested in a transient single point test to ensure the sinusoidal strain response followed the sinusoidal stress by a phase angle. Finally, a dynamic frequency sweep test was run at a constant stress over a frequency range of 0.01–10 Hz to determine both the real (storage elasticity) modulus, G', and the imaginary (loss) modulus, G''. For each sample, two sets of tests were run. The first set included the dynamic stress sweep test, the transient single point test, and the dynamic frequency sweep test. In the second set of tests, the sample was replaced with fresh sample from the same test tube and only the dynamic frequency sweep test was run. This second dynamic frequency sweep test was used to check the reproducibility of the first set of tests. In particular, we wished to ensure that the dynamic moduli were not merely products of alignment produced during the high stresses imposed by the dynamic stress sweep test.

F. Optical microscopy

Optical glass capillaries (Vitro Dynamics, Rockaway, NJ, USA) of thicknesses ranging from 0.05 to 0.2 mm were filled with sample and flame sealed. Some capillaries were cleaned first with a 2% solution of PCC-54 concentrate (Pierce, Rockford, IL, USA), then rinsed with spectroscopic grade ethanol, rinsed multiple times with Millipore water, dried and then subjected to 30–90 min of UV light in order to heighten the hydrophilicity of the glass, thus increasing the probability of homeotropic alignment. All samples were observed with an Optiphot 2-Pol microscope (Nikon, Torrance, CA, USA) using polarized light at different magnifications (50X–500X). Textures were photographed using an MFX-DX automatic camera and posemeter (Nikon, Torrance, CA, USA). The microscope was also equipped with an FP82 heating stage and an FP80 central processor (Mettler-Toledo Inc., Hightstown NJ, USA) for temperature annealing experiments.

FIG. 3. Series of test tubes filled with **1b** based mixtures of different compositions. From bottom to top increasing Φ_w. $c_{\text{PEG}}=[\text{mole PEG–surfactant}/(\text{mole PEG–surfactant}+\text{mole DMPC})]\times 100$. Bottom sample: $\Phi_w=0.72$ and $c_{\text{PEG}}=1.9$ in the fluid L_α-phase; second sample: $\Phi_w=0.78$ and $c_{\text{PEG}}=2.0$ in the $L_{\alpha,g}$ gel phase; third sample: $\Phi_w=0.85$ and $c_{\text{PEG}}=2.1$ in the $L_{\alpha,g}$ gel phase; top sample: $\Phi_w=0.92$ and $c_{\text{PEG}}=2.0$ in the two phase region.

III. RESULTS AND DISCUSSION

A. Visual inspection of test tubes

All samples are examined in test tubes in natural light to determine whether or not they are single phase. Biphasic samples will be turbid, and, if centrifuged long enough, will display a clear meniscus between the two phases. Samples are then also examined in polarized light to check for birefringence. In distinguishing between a fluid L_α phase and a $L_{\alpha,g}$ gel phase, any sample which does not flow for at least 5 s after inversion of the sample is labeled a gel. All samples are labeled according to these simple tests.

To illustrate this method, Fig. 3 shows a series of samples containing the PEG–surfactant **1b**. For all four samples, $c_{\text{PEG}}\approx 2.0\%$, but Φ_w increases from bottom to top. The test tubes have just been tilted in the horizontal position to demonstrate the different flow properties of the samples. The lowest water concentration sample flows as expected for a dilute L_α phase. As the water proportion increases, a threshold ($\Phi_w\approx 0.76$) is reached beyond which the samples do not flow any more, showing elastic properties instead (middle two samples). As the water content increases even more, the samples become turbid and biphasic, losing their gel behavior (top sample).

When examined between crossed polarizers, the bulk appearance of the samples from the two different L_α regimes is strikingly different. Samples from the L_α fluid phase are

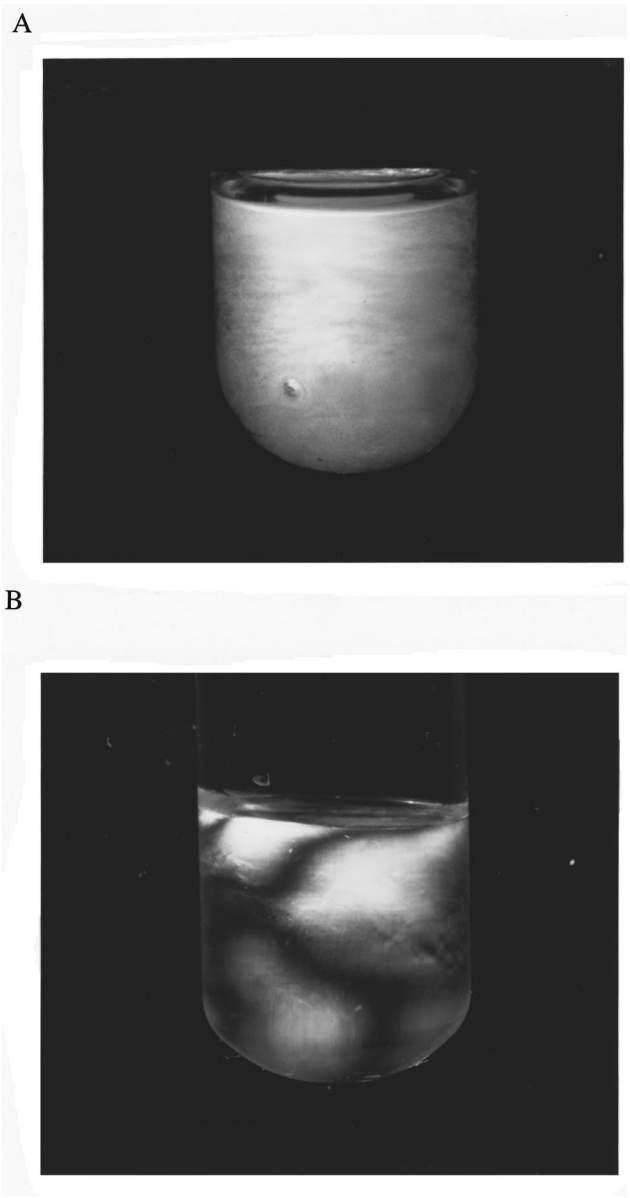

FIG. 4. Test tubes viewed between crossed polarizers. (a) **1b** based sample at $\Phi_w = 0.72$ and $c_{\mathrm{PEG}} = 1.9$ in the L_α fluid phase; (b) **1b** based sample at $\Phi_w = 0.85$ and $c_{\mathrm{PEG}} = 2.1$ in the $L_{\alpha,g}$ gel phase.

clearly birefringent but do not show any macroscopic texture [Fig. 4(a)]. In contrast, samples of the $L_{\alpha,g}$ gel phase generally show a nematiclike texture with a variable density of line-defects on a millimeter length scale [Fig. 4(b)]. Such samples, which appear clear and colorless in normal light, often display a brilliant variety of birefringence colors.

B. Phase diagrams

Figures 5(a)–5(d) show the phase diagrams obtained with compounds **1a**, **1b**, **2a**, and **2b**, respectively. In each case, the molar ratio of PEG–surfactant to total surfactant, c_{PEG}, was varied from 0 to 30%. Two phase boundaries at low and high water concentrations were identified for all compounds. The lower 2-phase boundary depends only slightly on c_{PEG} and occurs around 42%–45% water for compounds **1a** and **2a** [Figs. 5(a) and 5(c)] and around 64%–67% water for compounds **1b** and **2b** [Figs. 5(b) and 5(d)]. In terms of intermembrane spacing d, these values correspond to ~ 55 and 90 Å, respectively. Subtracting from this the membrane thickness of 26.4 Å (see Fig. 12), we find that the lamellar phase is stable only for water spacings greater than approximately 30 Å in the case of **1a**, **2a** and 63 Å for compounds **1b**, **2b**. The radius of gyration of a polyethylene glycol 2000 polymer–surfactant incorporated in lipid bilayers has been measured to be 25–35 Å.[17] Extrapolating this measurement to 5000 molecular weight polyethylene glycol via Flory arguments, one obtains an R_g of approximately 60 Å. We surmise therefore that the lamellar regimes are only stable when the water spacing exceeds the natural polymer extension. Thus the position of the lower two-phase boundary is independent of the substituent alkyl chain of the PEG–surfactant but strongly dependent on polymer molecular weight.

In contrast, for all four PEG–surfactants studied, the higher 2-phase boundary is reached around 80%–90% water at low $c_{\mathrm{PEG}}(\approx 5\%)$ and then decreases regularly with c_{PEG}. Both the high and low water content biphasic regions seem to arise from the coexistence of the lamellar phase with other isotropic phases which we did not specifically study.

All phase diagrams show the fluid L_α and gel $L_{\alpha,g}$ phases separated by a gelation line. The fluid–gel transition is approximately independent of the substituent alkyl chain length. However, there is a strong dependence on the molecular weight of the polymer moiety of the PEG–surfactant; both **1b** and **2b** (5000 MW PEG) gel at less than half the c_{PEG} required for **1a** and **2a** (2000 MW PEG). For each compound the same behavior is observed; less PEG–surfactant is needed to achieve gelation as water content increases. This immediately differentiates these gels from free polyethylene glycol–water mixtures wherein the polymer overlap concentration, denoted c^*, must be exceeded for gelation to occur. For the PEG–surfactants, gelation occurs at polymer and water concentrations which preclude the possibility of polymer entanglement as a gelation mechanism. In particular, the $L_{\alpha,g}$ phase occurs in mixtures with measured d-spacings of ~ 200 Å. This is 6(3) times the polymer R_g of polyethylene glycol 2000 (5000). Moreover, to produce a gel in free polyethylene glycol–water mixtures the polymer molecular weight must be very high ($\sim 10^6$ g/mol).[23]

The mushroom-brush transition, predicted to occur at monolayer coverage (the PEG–surfactant concentration at which polyethylene glycol ''mushrooms'' would begin to laterally overlap), can also be eliminated as a source of gelation. Using values given in the Experiment for the surfactant and cosurfactant headgroups, we calculate the expected monolayer coverage, c_{mono}, for these membranes,

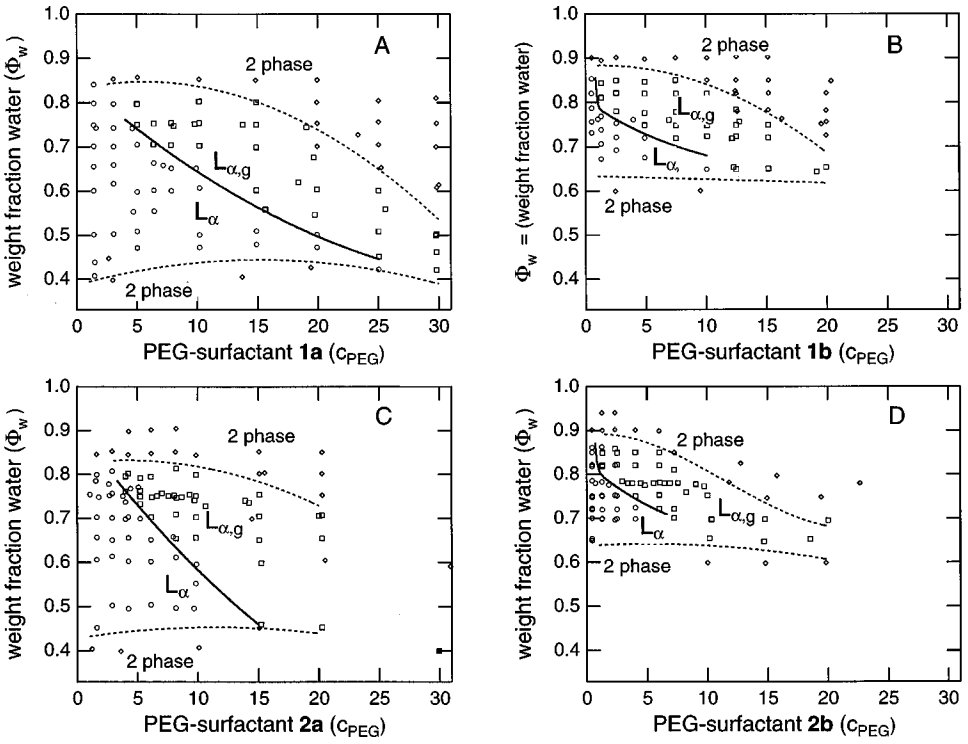

FIG. 5. Phase diagrams of polymer surfactants **1a**, **1b**, **2a**, and **2b** plotted in terms of the water weight fraction Φ_w vs c_{PEG}. c_{PEG} =[mole PEG–surfactant/(mole PEG–surfactant+mole DMPC)]×100. Molar ratio of pentanol to (DMPC+PEG–surfactant)=4:1. (a) Polymer surfactant **1a**; (b) polymer surfactant **1b**; (c) polymer surfactant **2a**; (d) polymer surfactant **2b**; ◇, two phase sample; □, gel with L_α-structure; ○, fluid with L_α-structure; —, fluid/gel transition; ---, single phase/two phase transition.

total membrane area

$$= 72.7\ \text{Å}^2 \times \left(\frac{g_{\text{PEG–surfactant}}}{\text{MW}_{\text{PEG–surfactant}}} + \frac{g_{\text{DMPC}}}{\text{MW}_{\text{DMPC}}} \right) + 12.8\ \text{Å}^2 \times \left(\frac{g_{\text{pent}}}{\text{MW}_{\text{pent}}} \right)$$

$$\approx 118\ \text{Å}^2 \times \left(\frac{g_{\text{PEG–surfactant}}}{\text{MW}_{\text{PEG–surfactant}}} + \frac{g_{\text{DMPC}}}{\text{MW}_{\text{DMPC}}} \right) \quad (8)$$

and

$$\text{mushroom area} = R_g^2 \times \left(\frac{g_{\text{PEG–surfactant}}}{\text{MW}_{\text{PEG–surfactant}}} \right), \quad (9)$$

therefore

$$c_{\text{mono}} \approx \frac{118}{R_g^2}. \quad (10)$$

For PEG–surfactants **1b** and **2b** (PEG molecular weight of 5000) c_{mono} is about 3 mol % and for PEG–surfactants **1a** and **2a**, c_{mono} is about 10 mol %. Note that gelation can be reached with c_{PEG} as low as 1 for compounds **1b** and **2b** and $c_{PEG} \approx 4$ for compounds **1a** and **2a**. We thus dismiss the influence of direct lateral interactions in the transition. We can also discount electrostatic interactions as the $L_{\alpha,g}$ phase forms as readily in brine as in water.[2]

C. Optical textures

Observed in flat glass capillary tubes with a polarizing microscope, samples of the fluid L_α phase show homeotropic regions separated by oily streak defects [striated lines, Fig. 6(a)] typical of L_α phases. A proposed structure[24] is shown in Fig. 6(d). The curved region is the bright oily streak defect (long axis parallel to OZ), and the flat well-aligned layers correspond to the homeotropic regions. After annealing a few days at room temperature, the density of oily streaks decreases markedly and homeotropic regions often develop the so-called parabolic texture [Fig. 6(a), arrow]. Some of these oily streaks are clearly chains of focal conic domains seen in similar L_α phases.[24,25]

In contrast, samples close to the fluid–gel transition line have a ''whispy'' texture [Fig. 6(b)], showing a large density of very thin linear defects reminiscent of the oily streak but lacking characteristic striations. A detailed freeze-fracture and optical microscopy study of similar samples[5] confirm the higher defect density relative to the fluid L_α phase. From that study, the microstructure comprises both spherulitic [Fig. 6(b), arrow] and oily-streak defects tethered together via shared membranes. These ''tethered defects,'' also observed in freeze-fracture images of $L_{\alpha,g}$ samples, are the probable source of the enhanced viscoelastic response. The overall linear, whispy texture shown in the transition sample [e.g. Fig. 6(b), asterisk] is consistent with the alignment of such defects through the shearing effect of drawing sample into a

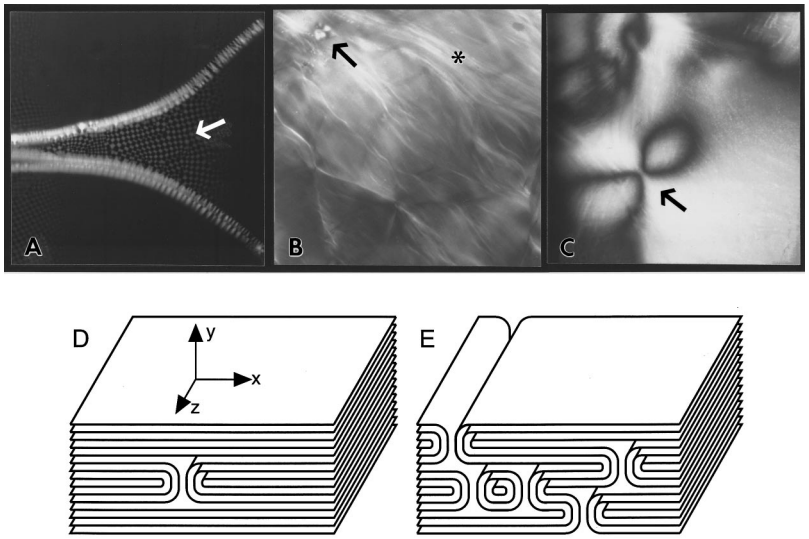

FIG. 6. Optical textures in polarized light. (magnification×100). (a) Sample at $\Phi_w=0.748$, $c_{\mathrm{PEG}}=0.45$ showing oily streaks and (arrow) parabolic focalconic array surrounded by homeotropic regions. (b) Sample at $\Phi_w=0.78$, $c_{\mathrm{PEG}}=4.5$ around the sol/gel transition showing the ''whispy'' texture (especially near asterisk) and a spherulite with an anisotropic cross (arrow). (c) Sample at $\Phi_w=0.78$, $c_{\mathrm{PEG}}=6.9$ in the $L_{\alpha,g}$ gel phase showing the nematic Schlieren texture (arrow).

thin optical capillary; it is probably incorrect to equate the whisps with oily streaks

Attempts to anneal away defects from transition or gel samples either at room temperature or by heating are unsuccessful to date. In fact, the inclusion of PEG–surfactant appears to extend the temperature range of stability of the lamellar phase. For example, in **1b** samples with $\Phi_w \sim 0.75$, the lamellar to isotropic temperature increases from around 40 °C for fluid samples (containing little PEG–surfactant) to greater than 100 °C for gel samples (more PEG-surfactant). Slowly cooling (-0.2 C/min) down through this transition effectively removes defects from the fluid samples, but in gel samples results in a reproliferation of defects as the lamellar phase reforms. Incubation of bulk gel samples at elevated temperatures for relatively long periods (e.g., 100 °C for several hours) does not appear to qualitatively affect the viscoelasticity; however, no quantitative rheometric tests were performed at elevated temperatures. Shearing gel samples between glass slide and cover slip also has little effect on sample texture, but does align samples from the fluid L_α phase.

Deeper in the gel region, samples become less and less birefringent. Whispy defects become denser and thinner, and finally a Schlieren texture [Fig. 6(c)] can be observed. This texture is very deceptive because, although four-brush Schlieren textures (strength+1) are observed in Smectic C phases, the texture of two brushes originating from a distinct center (i.e., strength+1/2) is associated with nematic phases.[25d] In the case of nematics, a point defect of strength+1 splits into a pair of defects of strength+1/2 [Fig. 6(c), arrow] for energetic reasons;[26,27] this phenomenon can be seen here under a rotation of the polarizer-analyzer system. However, in this case, x-ray scattering experiments described below show that the system remains lamellar, with a symmetry closest to that of the Smectic A phase. Inspection of this Schlieren texture reveals the existence of striations hardly resolvable by the optical microscope. These striations, generally not observed in the textures of nematic phases, are actually the aligned defects of the ''whispy'' texture which have become extremely thin and densely packed. These textures then probably indicate nematic ordering of defects on a length scale of a millimeter. Again, freeze-fracture images of analogous samples[5] confirm both the increase in defect density and decrease in size of individual defects in the gel regime; additionally, those images show the presence of regions of positive (spherulites) and negative (crescents) curvature. We propose the structure shown in Fig. 6(e); a dense, tightly packed collection of spherulitic and linear defects with few remaining well-aligned regions.

Optical capillary tubes filled with biphasic samples from both the low and high water regime usually show small bright droplets floating in an isotropic liquid. When the polarizers are removed, these droplets are still easily observed in natural light which reveals a clear boundary between two phases.

D. Rheology

Rheometric measurements were performed at room temperature on eight samples containing PEG–surfactant **1b**. These samples were chosen to span the observed qualitative behaviors from the L_α and $L_{\alpha,g}$ regimes. Four samples had c_{PEG} fixed at 5% with Φ_W increasing from 0.68 to 0.78 [Figs. 8(a)–8(d)]. The remaining four had Φ_W fixed at 0.76 while c_{PEG} increased from 1% to 10% [Figs. 9(a)–9(d)]. For all samples, two measurements of the real (elasticity) modulus G' and the imaginary (loss, viscosity) modulus G'' were made as described in the Experiment.

Figure 7 shows two such consecutive runs, in the same experimental conditions, for an L_α and $L_{\alpha,g}$ sample. Clearly

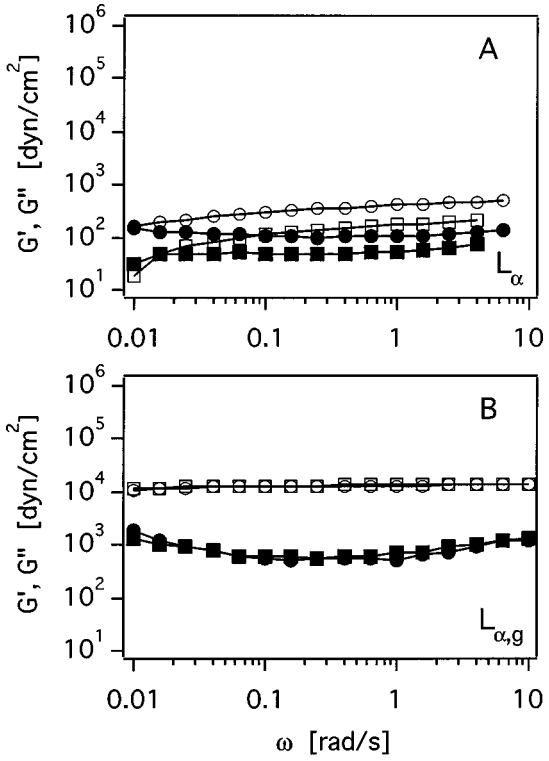

FIG. 7. Consecutive rheology experiments over a frequency range of 0.01–10 rad/s at room temperature. (a) Polymer surfactant **1b** at $\Phi_w = 0.72$ and $c_{\mathrm{PEG}} = 5$ in the fluid L_α phase. (b) Polymer surfactant **1b** at $\Phi_w = 0.78$ and $c_{\mathrm{PEG}} = 5$ in the $L_{\alpha,g}$ gel phase. G', open symbols; G'', filled symbols; □, ■, 1st run; ○, ●, 2nd run.

the data do not reproduce for the fluid lamellar sample [Fig. 7(a)]. This is understood by considering that fluid samples are in an anisotropic smectic phase initially in a macroscopically unoriented state (i.e., displaying an isotropic distribution of smectic domains) but prone to be oriented under shear flow so that different combinations of elastic constants and Miesowicz viscosities are involved for each run.[28,29] In other words, the applied shear stress is progressively able to remove topological defects present at the beginning of the experiment. The behavior of a gel sample is very different; consecutive runs do reproduce within experimental accuracy [Fig. 7(b)]. The applied shear stress cannot suppress the topological defects which may therefore be regarded as intrinsic to the gel phase. This observation is consistent with the failure of both heat and shear annealing to remove defects from $L_{\alpha,g}$ samples during polarizing microscopy studies.

Figure 8 shows data collected for samples of fixed c_{PEG} and increasing Φ_W. The bottom two samples, taken from the fluid L_α regime, display roughly comparable viscous and elastic moduli throughout the measured frequency range. At the lowest measured frequencies, the dynamic moduli appear to approach a crossover point unanticipated in fluids. However, this aspect of the data is unreliable for the reasons discussed in the preceding paragraph; subsequent experiments might produce a crossover at a significantly different frequency or show no crossover at all. In sharp contrast, the data from the two high-water gel samples shown in Figs. 8(c) and 8(d) show a G'/G'' ratio greater than 10 for all

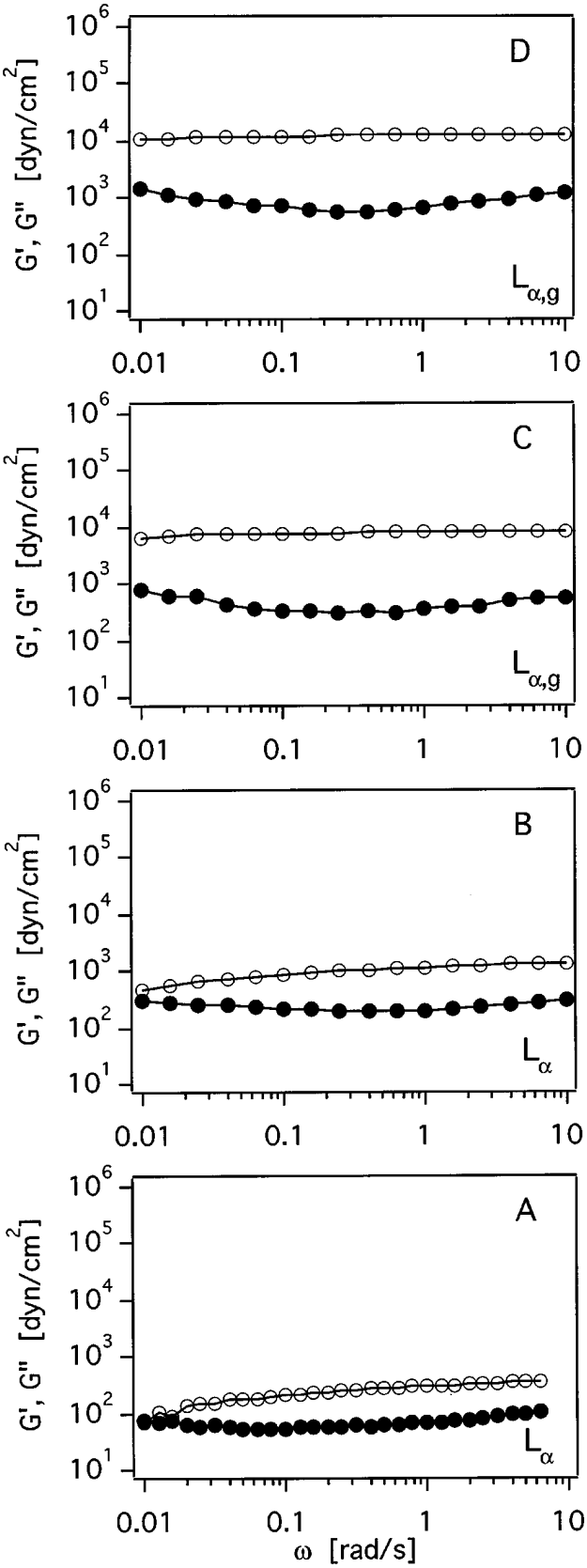

FIG. 8. Rheology experiments after an initial stress sweep over a frequency range of 0.01–10 rad/s at room temperature for different concentrations of Φ_w at constant polymer surfactant concentration $c_{\mathrm{PEG}} = 5$. (a) Polymer surfactant **1b** at $\Phi_w = 0.68$ in the fluid L_α phase; (b) polymer surfactant **1b** at $\Phi_w = 0.72$ in the fluid L_α phase; (c) polymer surfactant **1b** at $\Phi_w = 0.76$ in the $L_{\alpha,g}$ gel phase; (d) polymer surfactant **1b** at $\Phi_w = 0.78$ in the $L_{\alpha,g}$ gel phase.

frequencies. Although both moduli increased from the fluid values, G' has increased an order of magnitude more than the viscous modulus. The data resembles that from a chemical gel with no hint of crossover; however the reversible nature of the gel phase argues that the gel must be physical.

Data as a function of increasing c_{PEG} (Fig. 9) largely replicates that taken for the Φ_W line. The bottom sample, a fluid L_α phase, has $G' \sim G''$, while the top two, taken from the $L_{\alpha,g}$ regime display the strong elasticity ($G' > 10^* G''$) previously seen for gel samples in the water dilution line. However, the data of Fig. 9(b), from a fluid sample near the $L_\alpha - L_{\alpha,g}$ transition, displays gel characteristics even though this sample was classified as a fluid in the phase diagram. This discrepancy arises from the use of the ''sample inversion'' test to classify the large number of samples used in making the phase diagrams; i.e., only samples with yield stresses greater than their own weight were labeled gels. Relatively ''weak'' gels occurring in the transition region between the L_α and $L_{\alpha,g}$ phases would be labeled as fluids, although no fluids would be mistaken for gels.

While the inversion test may ''delay'' identification of the $L_\alpha - L_{\alpha,g}$ transition in terms of c_{PEG} or Φ_W from the values indicated by more quantitative tests, it should not alter the key characteristic discussed in this paper, the nature and general shape of the transition line. Moreover, this ambiguity does not affect arguments presented previously to eliminate either polymer entanglement or electrostatic interactions as a source of gelation. Finally, these rheometric experiments quantify the qualitative behavior illustrated in Fig. 3 and proves the existence of elastic, solidlike properties even in samples of very low PEG–surfactant and high water concentrations.

E. X-ray scattering: Evidence for a long-range repulsive interaction in flexible L_α phases with end-anchored polymer-lipids

Figure 10 shows a series of small angle, high resolution x-ray powder scans for PEG–surfactants **2a** and **2b**, split fairly evenly between L_α and $L_{\alpha,g}$ samples. In all scans, one observes a series of (00L) reflections due to the lamellar periodicity.

Figures 10(a) and 10(b) display spectra at constant Φ_W but increasing (bottom to top) c_{PEG} for the PEG–surfactants **2a** and **2b**, respectively. The number of harmonics increases regularly with c_{PEG}, indicating a direct dependence of elastic constants on PEG–surfactant concentration. Profiles of the (00L) reflections are described by power-law divergences of the form $S(q) \propto |q - q_{00L}|^{-p}$, where q_{00L} is the position of the $(00L)$ peak and p is an exponent which asymptotically close to q_{00L} is 1-η for ''powder'' samples.[7–9,30] The coefficient η is in turn given by the expression $\eta \propto (1/\sqrt{KB})$, where K is the splay elastic constant and B is the compressibility modulus of the lamellar phase. The observation of a given $(00L)$ reflection requires that the exponent p be positive;[30] thus an estimate of η can be obtained from the number of detected (00L) reflections. In this context, the behavior shown in Figs. 10(a) and 10(b) points to a decrease

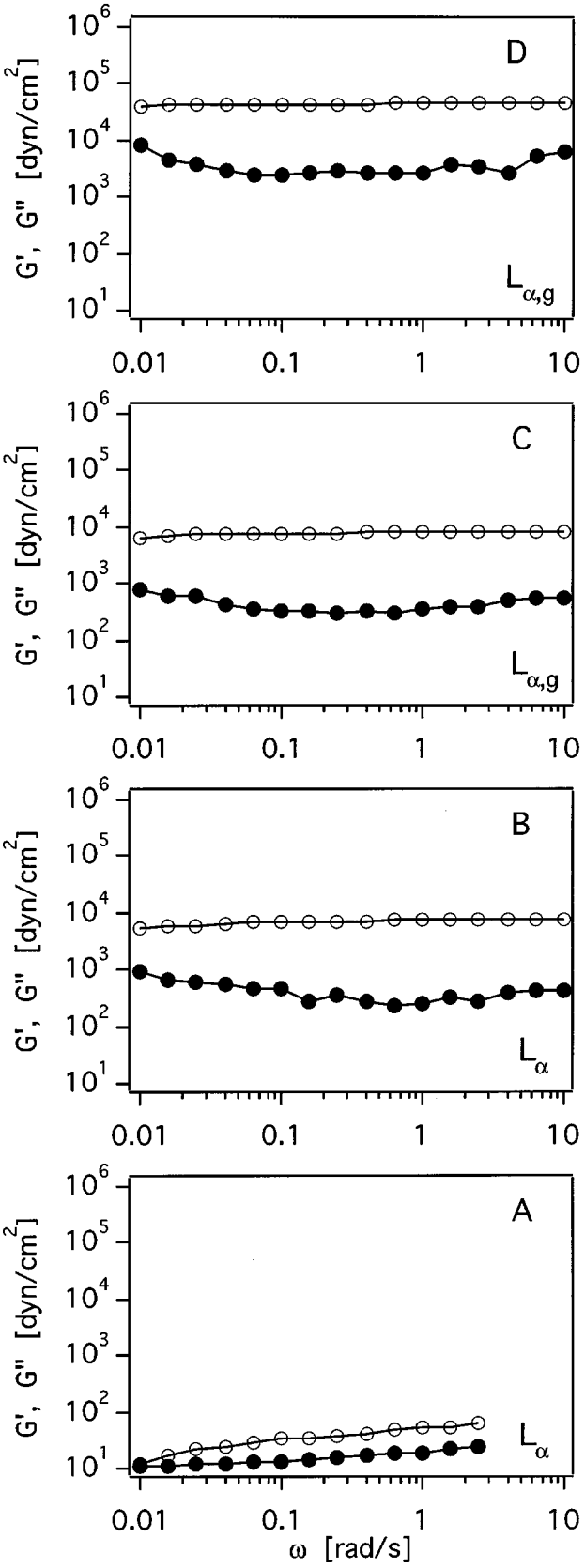

FIG. 9. Rheology experiments after an initial stress sweep over a frequency range of 0.01–10 rad/s at room temperature for different concentrations of c_{PEG} at constant $\Phi_w = 0.76$. (a) Polymer surfactant **1b** at $c_{\mathrm{PEG}} = 1$ in the fluid L_α phase; (b) polymer surfactant **1b** at $c_{\mathrm{PEG}} = 4$ in the fluid L_α phase; (c) polymer surfactant **1b** at $c_{\mathrm{PEG}} = 5$ in the $L_{\alpha,g}$ phase close to the transition to the fluid L_α phase; (d) polymer surfactant **1b** at $c_{\mathrm{PEG}} = 10$ in the $L_{\alpha,g}$ phase.

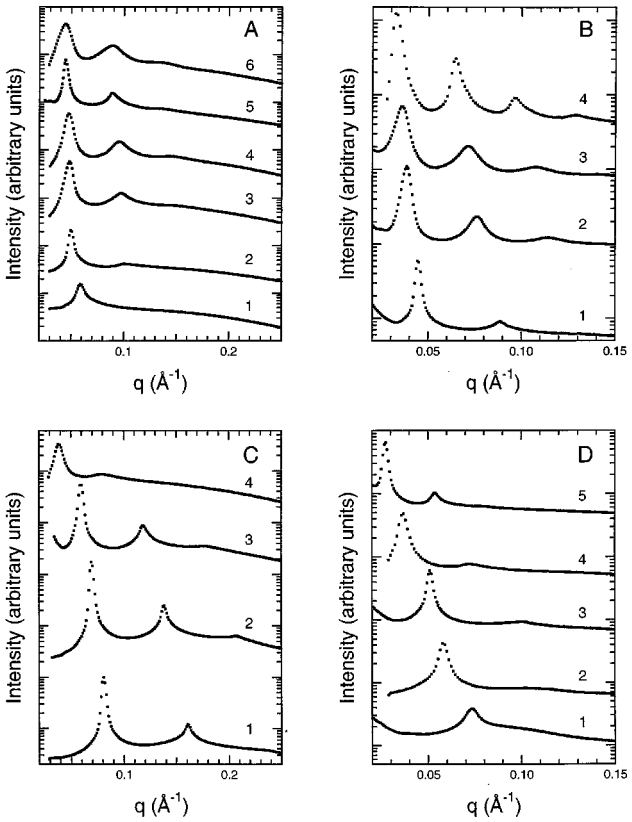

FIG. 10. X-ray small angle scans of unoriented samples. (a) Polymer surfactant **2a** at constant $\Phi_w=0.75$ and different c_{PEG} concentrations. (1) $c_{\mathrm{PEG}}=0$; (2) $c_{\mathrm{PEG}}=1.8$; (3) $c_{\mathrm{PEG}}=5.2$; (4) $c_{\mathrm{PEG}}=7.6$; (5) $c_{\mathrm{PEG}}=8.7$; (6) $c_{\mathrm{PEG}}=14.2$. (b) Polymer surfactant **2b** at constant $\Phi_w=0.78$ and different c_{PEG} concentrations. (1) $c_{\mathrm{PEG}}=1.8$; (2) $c_{\mathrm{PEG}}=3.8$; (3) $c_{\mathrm{PEG}}=6.1$; (4) $c_{\mathrm{PEG}}=9.1$. (c) Polymer surfactant **2a** at constant $c_{\mathrm{PEG}}=4.25$ and different Φ_w. (1) $\Phi_w=0.60$; (2) $\Phi_w=0.66$; (3) $\Phi_w=0.70$; (4) $\Phi_w=0.80$. (d) Polymer surfactant **2b** at constant $c_{\mathrm{PEG}}=0.45$ and different Φ_w. (1) $\Phi_w=0.65$; (2) $\Phi_w=0.72$; (3) $\Phi_w=0.75$; (4) $\Phi_w=0.82$; (5) $\Phi_w=0.86$.

by at least an order of magnitude of the coefficient η. Most of this decrease occurs at minute concentrations of PEG–surfactant, where the bending rigidity of the membrane should be basically unaffected; moreover, it is very unlikely in any case for K to increase by two orders of magnitude. We therefore believe that this variation of η reflects a large increase in the compressibility B caused by the PEG–surfactant. This stiffening of the compressibility at low polymer-lipid coverages points to a long-range repulsive interaction unrelated to the polymer-brush effect. Preliminary work indicates that this behavior may be attributed to an undulation-induced antidepletion interaction originating from the freely diffusing polymer chains anchored at the fluid membrane interface.[31]

However, no discontinuity is detected around the L_α–$L_{\alpha,g}$ transition region, making a connection between gelation and decreased compressibility unlikely. In addition, small angle x-ray powder scans along an increasing water line at constant PEG–surfactant concentration [Figs. 10(c) and 10(d)] show that the number of detected harmonics remains approximately constant across the L_α–$L_{\alpha,g}$ transition.

In each series of scans [Figs. 10(a)–10(d)], the peak

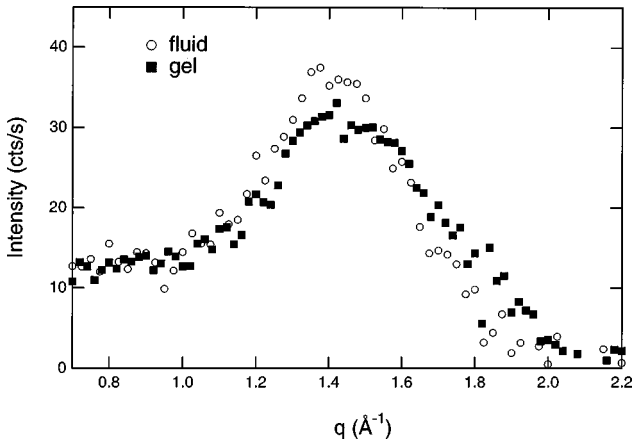

FIG. 11. X-ray wide angle scattering of □, a gel with L_α-structure (**1b**, $c_{\mathrm{PEG}}=10.1$, $\Phi_w=0.75$); ○, fluid with L_α-structure (**1b**, $c_{\mathrm{PEG}}=0.5$, $\Phi_w=0.73$).

width of the first harmonic undergoes a pronounced increase as the L_α–$L_{\alpha,g}$ transition is spanned. Comparing, for example, scans 10B1 (L_α) and 10B2 ($L_{\alpha,g}$), the peak width roughly doubles. Since peak width is inversely proportional to smectic domain size, this indicates a significant decrease in the average number of correlated layers in the gel regime as compared to the fluid regime, consistent with both the polarizing microscopy and rheometric observations of increased defect density in the $L_{\alpha,g}$ phase.

X-ray scattering at wide angles (Fig. 11) shows the liquidlike peak due to surfactant chains at $q\approx 1.4$ Å^{-1} for both L_α and $L_{\alpha,g}$ phases. The gel phase is thus comprised of fluid membranes in which the surfactant chains are in the molten state expected of L_α phases. Unlike $L_{\beta'}$ phases, gelation is not due to an in-plane chain ordering.

A plot of the lamellar period d versus the membrane volume fraction Φ_{mem}, when the solubility of pentanol in water (2.6%) is taken into account, shows the linear behavior expected for a purely one-dimensional lamellar system (Fig.

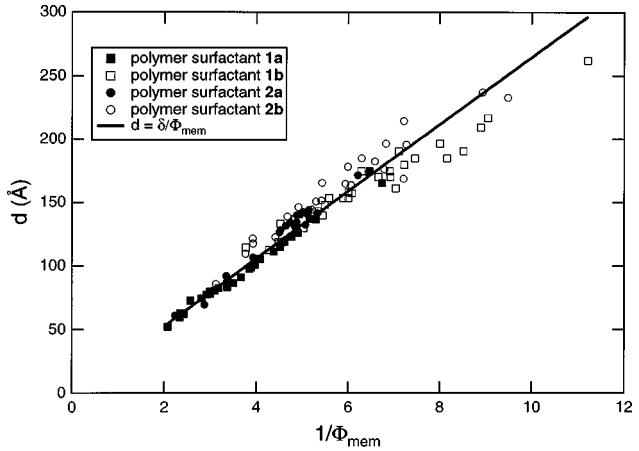

FIG. 12. Plot of the intermembrane spacing d vs $1/\Phi_{\mathrm{mem}}$, where Φ_{mem} is the ratio of the volume of DMPC, PEG–surfactant and the fraction of pentanol retained in the membrane to the total sample volume. From geometrical arguments, the slope of the plot must be equal to δ, the membrane thickness. $\delta=26.4\pm0.1$ Å, reduced $\chi^2=2.8$, number of points=100.

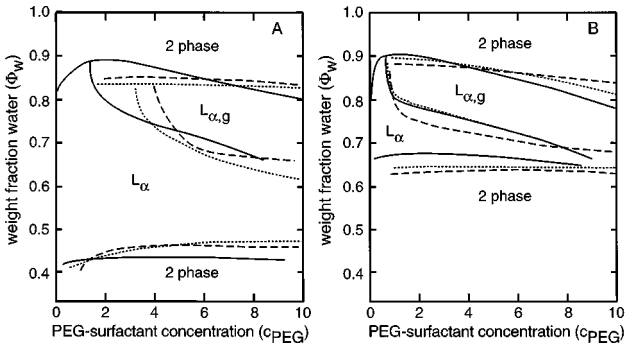

FIG. 13. (A) Schematics of phase boundaries for Avanti PEG2000 (—), PEG-surfactant **1a** (---), PEG–surfactant **2a** (···). (B) Schematics of phase boundaries for Avanti PEG5000 (—), PEG–surfactant **1b** (---), PEG–surfactant **2b** (···).

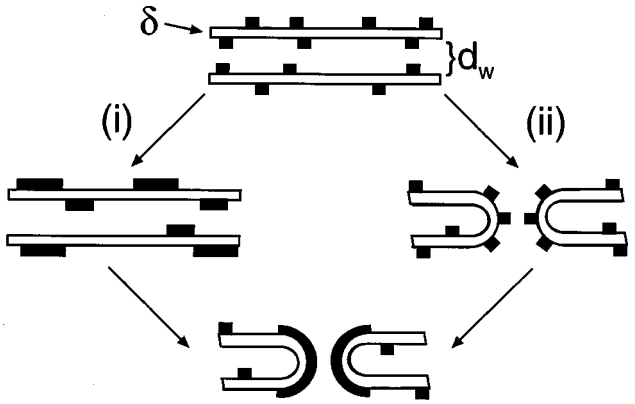

FIG. 14. Schematic of two paths that would form defects, with the laterally phase separated PEG–surfactant residing in, and stabilizing, the regions of high curvature.

12). Linear fits to the data provide the membrane thickness $\delta = 26.4 \pm 0.1$ Å. Within experimental accuracy, membrane thickness depends neither on the nature of the PEG–surfactant nor on c_{PEG}. This value therefore represents the thickness of the bare membrane made of DMPC and pentanol, in fair agreement with earlier values of about 28 Å.[7]

F. Comparison between the PEG–surfactants 1a, 1b, 2a, 2b and PEG–surfactant

Schematics of phase diagrams previously obtained[1,2] with the two polymer–surfactants PEG2000–DMPE and PEG5000–DMPE are shown in Fig. 13 together with those for the PEG–surfactants studied here. Inspection shows that the phase diagrams of compounds **1b** and **2b** can almost be superposed on that of PEG5000–DMPE. In the same way, the phase diagrams of compounds **1a** and **2a** approximate that of PEG2000–DMPE, although the upper and lower two-phase boundaries show better agreement than the fluid–gel transition line. Differences are most striking at very low c_{PEG}; possibly the Avanti polyethylene glycol 2000 had a somewhat larger MW than the batch used to make PEG–surfactants **1a** and **2a**, resulting in gelation at lower c_{PEG}. We also note that small variations in polymer molecular weights would be most apparent in comparisons of the lowest MW polymer–surfactants, where $\Delta N/N$ is greatest.

All six polymer–surfactants induce the occurrence of the $L_{\alpha,g}$ phase in the same way; less PEG–surfactant is needed to achieve gelation as water content increases. Moreover, polymer–surfactants containing 5000 MW polyethylene glycol uniformly produce gelation at lower c_{PEG} than those containing 2000 MW polyethylene glycol. This comparison demonstrates that the polymerization degree N is the main parameter governing the onset of the $L_{\alpha,g}$. Within our range of variation, perhaps because of the low PEG–surfactant concentrations used, the precise chemical nature of the hydrophobic grafted moiety does not appreciably influence the physical properties of the phase. Indeed, the similarity of behavior observed with different PEG–surfactants suggests that a general process, not involving molecular details, should be able to describe the gel transition of this 1d ordered material.

G. Description of the gel transition

Any model of this transition should at least account for the unusual inverse relationship between Φ_W and c_{PEG} observed along the gel transition line and predict the scaling dependence of the interlayer spacing at the gel transition on PEG molecular weight. We have shown in previous sections that the gel transition does not proceed from the usual mechanisms of polymer chain entanglements or in plane surfactant chain ordering which occur in common polymer physical gels and $L_{\beta'}$ phases, respectively. Microscopic observations indicate that a proliferation of tethered topological defects is associated with the gel transition. Rheological data presented here imply that these defects are intrinsic to the gel phase, while the x-ray spectra show a consistently decreased domain size (increased defect density) in the $L_{\alpha,g}$ phase compared to the L_α.

Topological defects are expected to arise because the PEG–surfactants are highly asymmetrical molecules (Fig. 1) and should tend either to create, or to segregate into, curved membrane regions. Membranes composed solely of DMPC and pentanol have a zero spontaneous curvature $C_0^L = 0$ (Refs. 1, 2, 7), whereas the PEG–surfactant favors a nonzero spontaneous curvature $C_0^P > 0$. This intrinsic frustration should drive the nucleation and proliferation of defects. Nucleation may happen along two separate paths (Fig. 14). Along path (i), PEG–surfactant molecules first laterally segregate within their membranes, forcing these aggregation regions to curve and nucleate defects. Lateral phase separation has already been observed in PEG–surfactant monolayers spread at an air–water interface.[32] Along path (ii), recent theoretical work has shown that direct coupling between membrane curvature and the local concentrations of membrane components can lead to a curvature-induced in-plane phase separation resulting in stable defects.[33–36]

Let us now sketch the mechanical properties of defects. A defect free lamellar phase has a finite elasticity modulus for shear stresses applied along the normal to the layers, because of the energetically unfavorable tilting of the layers. The effect of defects is to introduce portions of layers which are oriented along other directions and which will therefore

resist any applied shear stresses along these directions, giving rise to a 3D elasticity. Tethering membranes observed in the freeze-fracture images would tend to enhance this effect; one can argue that the gel transition proceeds from the percolation of connected membrane bilayers which on a semimacroscopic length scale leads to domains of random layer orientation. This situation is similar to that theoretically described[37] in lamellar block-copolymer systems. These systems were indeed predicted to show 3D elastic properties because domains that have layer normals with a finite projection along the flow direction will resist shear.

We develop our model of the $L_\alpha - L_{\alpha,g}$ transition in terms of the oily streak, one of the more mathematically tractable defect geometries frequently observed in transition and gel samples. Consider the simple line-defect shown in Fig. 14, which is basically a channel linking two next neighbor $(n-1,\ n+1)$ water layers. The channel consists of an undulating pair of edge dislocations of opposite Burgers vectors ± 2, has a persistence length ξ_p, a total length L and an edge curvature $C=2/d$. The elastic deformation energy associated with such a defect can be calculated from the Helfrich elastic energy of fluid membranes,[8]

$$E_{\mathrm{el}}=\frac{1}{2}\,\kappa\int\left[(C_1-C_0)+(C_2-C_0)\right]^2 dS. \tag{11}$$

The principal curvatures are $C_1=2/d$ and $C_2=0$ which leads to

$$E_{\mathrm{el}}=\frac{1}{2}\,\kappa\left(\frac{2}{d}-C_0\right)^2 \pi L d. \tag{12}$$

Now, the line defect has a persistence length ξ_p along its main axis given by[38]

$$\xi_p=\frac{\pi d\kappa}{k_B T}. \tag{13}$$

The entropic contribution to the free energy is then given by

$$\mathrm{TS}=\frac{(k_B T)^2 L}{\pi d\kappa}. \tag{14}$$

Proliferation of these line defects will occur when the entropic contribution compensates the elastic energy,

$$\frac{\pi\kappa L d_{\mathrm{gel}}}{2}\left(\frac{2}{d_{\mathrm{gel}}}-C_{0_{\mathrm{gel}}}\right)^2=\frac{(k_B T)^2 L}{\pi d_{\mathrm{gel}}\kappa}, \tag{15}$$

which leads to

$$d_{\mathrm{gel}}=\frac{1}{C_{0_{\mathrm{gel}}}}\left[2-\frac{\sqrt{2}k_B T}{\pi\kappa}\right].$$

In a mean-field approximation, valid for a dilute ''gas'' of the PEG–surfactant, the spontaneous curvature C_0 of the membrane is proportional to both C_0^P and the global volume fraction of the PEG–surfactant in the membrane, Φ_V^{PEG}, so that the relation between the lamellar spacing d_{gel} along the gelation line and Φ_V^{PEG} finally reads

$$d_{\mathrm{gel}}=\frac{2-\dfrac{\sqrt{2}k_B T}{\pi\kappa}}{\phi_{V_{\mathrm{gel}}^{\mathrm{PEG}}} C_0^P}. \tag{16}$$

The volume fraction of the PEG–surfactant is proportional to the PEG–surfactant polymerization degree N and c_{PEG} while d is proportional to Φ_w; thus Eq. (16) is consistent with the observed inverse relationship between $\Phi_{w_{\mathrm{gel}}}$ and c_{PEG}. It is also possible to extract the dependence of $\Phi_{w_{\mathrm{gel}}}$ on N using a result derived for asymmetric diblock copolymers. The PEG–surfactants considered in this study can be regarded as highly asymmetric block copolymers of a special kind. The spontaneous curvature of an asymmetric block copolymer located on a spherical vesicle interface is given by[39]

$$C_0^P=\frac{2\epsilon\pi^{2/3}a^2}{12^{1/3}(1+3\epsilon^2)N^{2/3}\chi^{1/6}\nu}, \tag{17}$$

where ϵ, the asymmetry parameter for the PEG - molecule, is

$$\frac{1}{2}-\frac{\text{phobic length}}{\text{total length}},$$

a,ν are the length and volume of a PEG monomer, respectively, and χ is the Flory–Huggins parameter for PEG in water. Thus $C_0^P\propto 1/N^{2/3}$. This leads to the scaling law $\Phi_{w_{\mathrm{gel}}}\propto 1/N^{1/3}$. Qualitatively, this scaling law is consistent with the observations that, increasing the water content at fixed c_{PEG}, compounds **1b** and **2b** gel before compounds **1a** and **2a**.

Quantitative comparisons are also possible if we formally re-express Eq. (16) in terms of Φ_w and c_{PEG}. Using Eqs. (4)–(7), (16), and the condition that there are always approximately four times as many pentanol molecules as surfactant molecules and the approximation $\Phi_{\mathrm{mem}}\approx 1-\Phi_w$, we obtain

$$\Phi_{w_{\mathrm{gel}}}\cong 1-\frac{C_0^P\delta\left(\dfrac{\mathrm{MW_{PEG}}}{\rho_{\mathrm{H_2O+PEG}}}+\dfrac{\mathrm{MW_{phobic}}}{\rho_{\mathrm{phobic}}}\right)}{\left(2-\dfrac{\sqrt{2}k_B T}{\pi k}\right)\left(\dfrac{\mathrm{MW_{DMPC}}}{\rho_{\mathrm{DMPC}}}+4\,\dfrac{\mathrm{MW_{pent}}}{\rho_{\mathrm{pent}}}\right)}\,c_{\mathrm{PEG}_{\mathrm{gel}}} + O(c_{\mathrm{PEG}_{\mathrm{gel}}}^2) \tag{18}$$

which can be directly compared with the phase diagrams of the four PEG–surfactants. In this expression, only κ, the membrane bending rigidity is an adjustable parameter.

Figure 15 shows the fitted transition curves for each phase diagram. Because the model expression is valid for a dilute, noninteracting gas of PEG–surfactant molecules, only concentrations below c_{mono} were used. The transition points (solid symbols with error bars) used in performing the fit are calculated values made by averaging the Φ_w and c_{PEG} values of the fluid and gel samples closest to the transition region; i.e., for each transition point,

$$\Phi_{w_{\mathrm{gel}}}=\frac{\left(\Phi_{w_{L_{\alpha,g}}}+\Phi_{w_{L_\alpha}}\right)}{2},$$

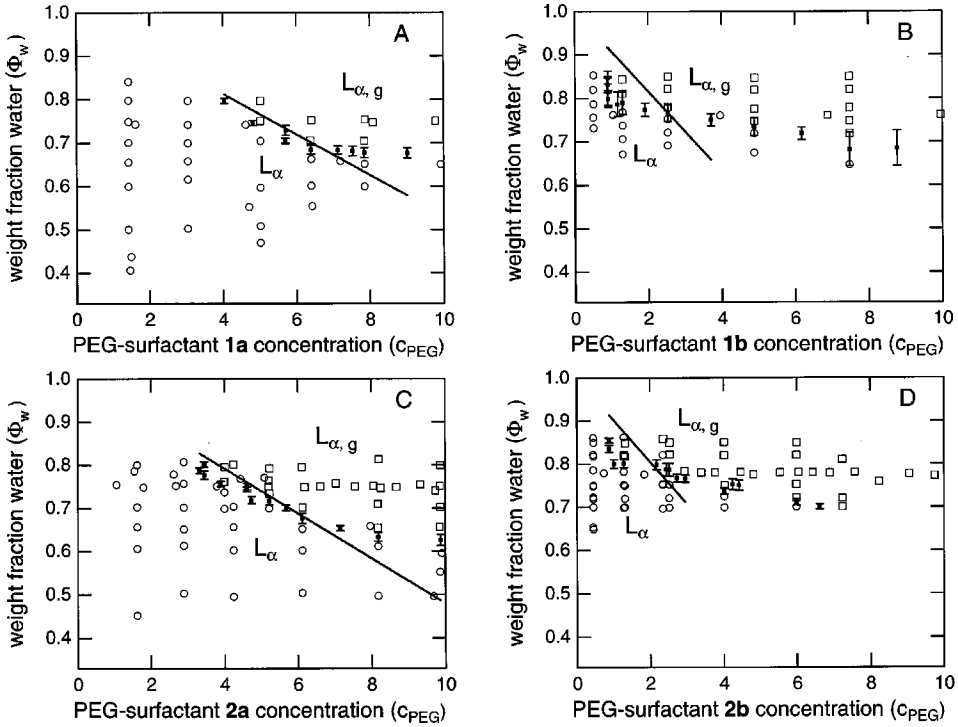

FIG. 15. Comparison of the fluid–gel transition model for $c_{PEG} \leqslant c_{mono}$ to the $\Phi_W - c_{PEG}$ phase diagrams of compounds **1a**–**2b**. —, fit to model; □, gel with L_α-structure; ○, fluid with L_α-structure; filled squares with error bars are the calculated fluid/gel transition points. (a) Polymer surfactant **1a**, reduced $\chi^2 = 35.6$, $m = 13.3 \pm 0.1$, number of points = 9. (b) Polymer surfactant **1b**, reduced $\chi^2 = 22.3$, $m = 14.2 \pm 0.5$, number of points = 12. (c) Polymer surfactant **2a**, reduced $\chi^2 = 27.8$, $m = 11.9 \pm 0.1$, number of points = 8. (d) Polymer surfactant **2b**, reduced $\chi^2 = 54.5$, $m = 13.6 \pm 0.2$, number of points = 8.

the water concentration at the transition point,

$$c_{PEG} = \frac{\left(c_{PEG_{L_{\alpha,g}}} + c_{PEG_{L_\alpha}}\right)}{2},$$

the PEG–surfactant concentration at the transition point,

$$\delta\Phi_{w_{gel}} = \sqrt{\frac{0.02^2}{2} + \frac{\left(\Phi_{w_{L_{\alpha,g}}} - \Phi_{w_{L_\alpha}}\right)^2}{4}},$$

the estimated uncertainty in $\Phi_{w_{gel}}$. It is clear that quantitative agreement is poor. In particular, reduced χ^2 values (22–55) indicate that the model expression does not capture all the important features of this transition. This is not unexpected; for example, there is the previously discussed ambiguity in the method used to classify fluid and gel samples, tending to increase the error in identifying transition points. Additionally, the model itself is overly simplified; a more complete model, taking into account both the lower stability limit in the phase diagram and the many other defect geometries observed in the $L_{\alpha,g}$ structure would doubtless have more success. We emphasize, however, that the present model does produce the correct general relationship between Φ_w and c_{PEG} at the transition and even allows reasonable estimates of the membrane bending rigidity κ. Taking $\chi = 0.23$ (Ref. 40), $\nu \cong 57$ Å^3 (Ref. 41), $a \equiv \nu^{1/3}$, and $\epsilon = (\delta/2)/(\delta/2 + R_g)$; for compounds **1a,2a** $\epsilon = 0.32$; for compounds **1b,2b** $\epsilon = 0.19$ in the C_0^P calculation, one finds, for all the PEG–surfactant systems, a κ of about $0.3 k_B T$. This value, lower than the value for a bare DMPC–pentanol membrane, is consistent with theoretical arguments that small quantities of asymmetric molecules lower κ for membranes of mixed composition.[33–35,39] It is also at the low end of theoretically permissible values of κ for an undulation-stabilized L_α phase.

IV. SUMMARY AND CONCLUSIONS

Four polymer–surfactant macromolecules, each consisting of a double chain hydrophobic moiety of different molecular weight attached to a polyethylene glycol (PEG) polymer chain, were synthesized in order to study the effects of their addition to the fluid lamellar liquid crystalline L_α, phase of the dimyristoylphosphatidylcholine (DMPC), pentanol, water system. The main finding of this study is that they induce the occurrence of a new lamellar gel phase, called $L_{\alpha,g}$. We presented the phase diagram of each PEG-surfactant molecule as a function of PEG–surfactant concentration, c_{PEG}, and water weight fraction Φ_w. All phase diagrams are qualitatively similar and show the existence of this physical gel. The gel transition is observed not only by increasing c_{PEG} but also by adding water at constant c_{PEG} an observation in contrast with the behavior of conventional polymer physical gels.

Small angle x-ray scattering experiments demonstrate the lamellar symmetry of the gel phase and also show that the number of smectic reflections regularly increases with

c_{PEG}. This increase is not correlated with the gel transition however. Wide angle x-ray scattering experiments prove the molten state of the lipid chains, differentiating the $L_{\alpha,g}$ phase from $L_{\beta'}$ phases. The $L_{\alpha,g}$ shows the rheological behavior of a gel, with an elastic modulus G' an order of magnitude larger than the loss modulus G'' throughout the gel regime. The $L_{\alpha,g}$ phase thus has the symmetry of an L_{α} phase but displays three-dimensional elasticity.

At the gel transition, polarized light microscopy reveals the proliferation of ''whispy'' defects reminiscent of oily streaks. Deeper in the gel regime, a nematiclike Schlieren texture can be observed, probably indicative of a nematic ordering of defects. Freeze fracture images demonstrate clearly that the $L_{\alpha,g}$ phase comprises a wide variety of interconnected spherulitic and layer-dislocation defects;[5] we infer that PEG–surfactant, aggregating in the high curvature regions, promotes and stabilizes this highly defected microstructure. Since domains with a layer normal along the direction of flow must resist shear, this semirandom orientation of domains leads to the observed gel-like elasticity.

The model of channel defects created by the lateral phase separation of PEG–surfactant into highly curved regions of the membranes is in good qualitative agreement with observed phase boundaries, but does poorly at describing the phase transition in detail. However, the model predicts both the inverse relationship between Φ_w and c_{PEG} observed along the gel transition line and the scaling dependence of the interlayer spacing at the gel transition with the PEG molecular weight. In addition, the model provides a reasonable estimate of the membrane bending rigidity κ.

These fluid membrane-based hydrogels suggest new directions for bioactive materials. Because the principle components are biocompatible, ''bioactive gels'' useful in tissue healing, chemical sensing, or drug delivery applications may be envisioned. In particular, $L_{\alpha,g}$ materials could provide mechanically strong and processable matrices capable of preserving the functionality of membrane proteins, peptides or other useful membrane-soluble molecules.

ACKNOWLEDGMENTS

We acknowledge useful discussions with P. Pincus. The work was partially supported by NSF Grant No. DMR-9624091, the Petroleum Research Fund (No. 31352-AC7). The Materials Research Laboratory at Santa Barbara is supported by the NSF under Grant No. DMR-96-32716. Hans-Werner Schmidt is especially grateful to the Visiting Research Fellowship from the Materials Research Laboratory. Synchrotron Experiments were carried out at Stanford (SSRL) which is supported under the U.S. D.O.E.

[1] H. E. Warriner, S. H. J. Idziak, N. L. Slack, P. Davidson, and C. R. Safinya, Science **271**, 969 (1996).
[2] H. E. Warriner, S. H. J. Idziak, N. L. Slack, P. Davidson, and C. R. Safinya (unpublished).
[3] (a) A. Tardieu, V. Luzzati, and F. C. Reman, J. Mol. Biol. **75**, 711 (1973); (b) D. M. Small, in *Handbook of Lipid Research* (Plenum, New York, 1986), Vol. 4; (c) G. S. Smith, E. B. Sirota, C. R. Safinya, and N. A. Clark, Phys. Rev. Lett. **60**, 813 (1988); (d) G. S. Smith, E. B. Sirota, C. R. Safinya, R. J. Plano, and N. A. Clark, J. Chem. Phys. **92**, 4519 (1990).
[4] S. Saeki, N. Kuwahara, M. Nakata, and M. Kaneko, Polymer **17**, 686 (1976).
[5] S. L. Keller, H. E. Warriner, C. R. Safinya, and J. A. N. Zasadzinski, Phys. Rev. Lett. **78**, 4781 (1997).
[6] (a) C. Ligoure, G. Bouglet, and G. Porte, Phys. Rev. Lett. **71**, 3600 (1993); (b) M. Singh, R. Ober, and M. Kleman, J. Phys. Chem. **97**, 11 108 (1993); (c) E. Z. Radlinska, T. Gulik-Krzywicki, F. Lafuma, D. Langevin, W. Urbach, C. E. Williams, and R. Ober, Phys. Rev. Lett. **74**, 4237 (1995); (d) M. F. Ficheux, A. M. Bellocq, and F. Nallet, J. Phys. II France **5**, 823 (1995); (e) B. Deme *et al.*, J. Phys. Chem. **100**, 3828 (1996).
[7] C. R. Safinya, E. B. Sirota, D. Roux, and G. S. Smith, Phys. Rev. Lett.**62**, 1134 (1989).
[8] (a) W. Helfrich, Z. Naturforsch. A **33**, 305 (1978); (b) Z. Naturforsch. C **28**, 693 (1973).
[9] C. R. Safinya *et al.*, Phys. Rev. Lett. **57**, 2718 (1986).
[10] N. A. Peppas and R. Langer, Science **263**, 1715 (1994).
[11] See, for example (a) *Peptide and Protein Drug Delivery*, edited by V. H. L. Lee (Dekker, New York, 1991); (b) E. Marshall, Science **269**, 1050 (1995).
[12] (a) T. M. Allen and A. Chonn, FEBS Lett. **223**, 42 (1987); (b) A. Gabizon and D. Papahadjopoulos, Proc. Natl. Acad. Sci. USA **85**, 6949 (1988).
[13] D. D. Lasic, *Liposomes: From Physics to Applications* (Elsevier, Amsterdam, 1993).
[14] See, for example (a) D. D. Lasic and D. Papahadjopoulos, Science **267**, 1275 (1995); (b) *Stealth Liposomes*, edited by D. D. Lasic and F. J. Martin (Chemical Rubber, Boca Raton, 1995).
[15] (a) S. Alexander, J. Phys. France **38**, 977 (1977); (b) P. G. De Gennes, *ibid*. **37**, 1443 (1976); (c) Macromolecules **13**, 1069 (1980); (d) S. T. Milner, Science **251**, 905 (1991).
[16] (a) D. Needham, T. J. McIntosh, and D. D. Lasic, Biochim. Biophys. Acta **1108**, 40 (1992); (b) A. K. Kenworthy, K. Hristova, D. Needham, and T. J. McIntosh, Biophys. J. **68**, 1921 (1995).
[17] T. L. Kuhl, D. E. Leckband, D. D. Lasic, and J. N. Israelachvili, Biophys. J. **66**, 1479 (1994).
[18] See, for example *Polymer Gels: Fundamentals and Biomedical Applications*, edited by D. DeRossi, K. Kajiwara, Y. Osada, A. Yamauchi (Plenum, New York, 1991).
[19] Petra Eiselt, Matthias Schellhorn, Hans Werner Schmidt, and Cyrus R. Safinya (in preparation).
[20] H. Träuble and D. H. Haynes, Chem. Phys. Lipids **7**, 324 (1971).
[21] P. Gonzalez-Tello, F. Camacho, and G. Blazquez, J. Chem. Eng. Data **39**, 611 (1994).
[22] *Solubilities of Inorganic and Organic Compounds*, edited by H. Stephen and T. Stephen (Pergamon, New York, 1963–79), Vol. 1, part 1, p. 418.
[23] F. E. Bailey and J. V. Koleske, *Poly(ethylene) Oxide* (Academic, New York, 1976).
[24] (a) S. A. Asher and P. S. Pershan, Biophys. J. **27**, 393 (1979); (b) M. B. Schneider and W. W. Webb, J. Phys. France **45**, 273 (1984).
[25] (a) P. Boltenhagen, M. Kleman, and O. Lavrentovich, C. R. Acad. Sci. Paris II **315**, 931 (1992); (b) P. Boltenhagen, O. Lavrentovich, and M. Kleman, Phys. Rev. A **46**, R1743 (1992); (c) P. Boltenhagen, M. Kleman and O. Lavrentovich, J. Phys. II France **4**, 1439 (1994); (d) G. W. Gray and J. W. G. Goodby, *Smectic Liquid Crystals* (Leonard Hill, New York, 1984).
[26] P. G. De Gennes and J. Prost, *The Physics of Liquid Crystals*, 2nd ed. (Clarendon, Oxford, 1993).
[27] M. Kleman, *Points, Lines and Walls in Liquid Crystals, Magnetic Systems and Various Ordered Media* (Wiley, New York, 1983).
[28] C. R. Safinya, E. B. Sirota, R. F. Bruinsma, C. Jeppesen, R. J. Plano, and L. J. Wenzel, Science **261**, 588 (1993).
[29] C.-Y. D. Lu and M. E. Cates, J. Chem. Phys. **101**, 5219 (1994).
[30] A. Caille, Comptes Rendus Hebdomadaires des Seances de l'Academie des Sciences, Serie B **274**, 891 (1972).
[31] H. E. Warriner, C. R. Safinya, and P. Pincus (in preparation).
[32] B. H. Cao and M. W. Kim, Faraday Discuss **98**, 245 (1994).

[33] S. Leibler, J. Phys. (France) **47**, 507 (1986).
[34] R. Liposky, Biophys. J. **64**, 1133 (1993).
[35] U. Seifert, Phys. Rev. Lett. **70**, 1335 (1993).
[36] T. Kawakatsu, D. Andelman, K. Kawasaki, and T. Taniguchi, J. Phys. II France **3**, 971 (1993).
[37] K. Kawasaki and A. Onuki, Phys. Rev. A **42**, 3664 (1990).
[38] W. Helfrich and W. Harbich, Chem. Scr. **25**, 2 (1985); also independently calculated by F. MacKintosh (private communication).
[39] Z. G. Wang and S. Safran, J. Phys. France **51**, 185 (1990).
[40] Y. C. Bae *et al.*, J. Appl. Polym. Sci. **47**, 1193 (1993).
[41] G. T. Dee *et al.*, Polymer **33**, 3462 (1992); G. C. Berry and T. G. Fox, Adv. Polym. Sci. **5**, 261 (1968).